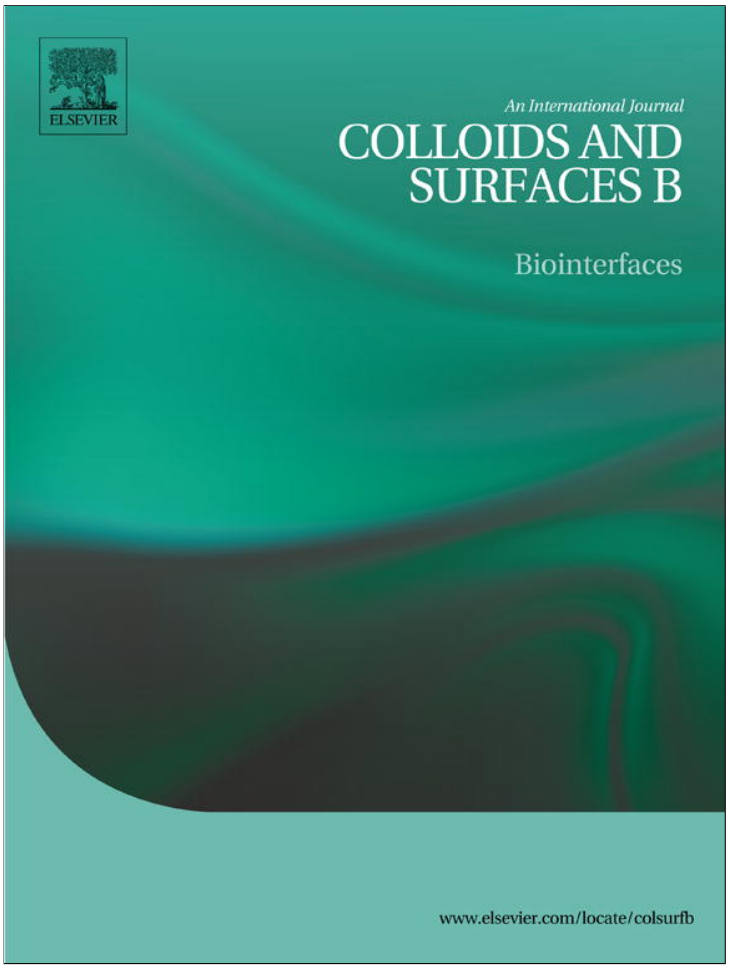

(This is a sample cover image for this issue. The actual cover is not yet available at this time.)

Colloids and Surfaces B: Biointerfaces 102 (2013) 218–226

Contents lists available at SciVerse ScienceDirect

Colloids and Surfaces B: Biointerfaces

journal homepage: www.elsevier.com/locate/colsurfb

Polyphenol–SiO_2 hybrid biosorbent for heavy metal removal. Yerba mate waste (*Ilex paraguariensis*) as polyphenol source: Kinetics and isotherm studies

G.J. Copello[a,b], M.P. Pesenti[a], M. Raineri[a], A.M. Mebert[a], L.L. Piehl[c], E. Rubin de Celis[c], L.E. Diaz[a,b,*]

[a] *Cátedra de Química Analítica Instrumental, Facultad de Farmacia y Bioquímica, Universidad de Buenos Aires (UBA), Junín 956, C1113AAD Buenos Aires, Argentina*
[b] *IQUIMEFA (UBA-CONICET), Junín 956, C1113AAD Buenos Aires, Argentina*
[c] *Cátedra de Física, Facultad de Farmacia y Bioquímica, Universidad de Buenos Aires (UBA), Junín 956, C1113AAD Buenos Aires, Argentina*

ARTICLE INFO

Article history:
Received 8 March 2012
Received in revised form 13 July 2012
Accepted 6 August 2012
Available online xxx

Keywords:
Sol–gel
Ilex paraguariensis
Polyphenol
Low-cost biosorbent
Metal removal
Hybrid material

ABSTRACT

A low-cost biosorbent hybrid material ready for application was obtained in this work. Yerba mate (*Ilex paraguariensis*) milling residual dust was used as a polyphenol source by ethanolic extraction. Polyphenols were immobilized within a SiO_2 matrix to form an interpenetrated polymer after glutaraldehyde cross-linking. Pb(II), Cr(III) and Cr(VI) were chosen as model metals for adsorption. The hybrid materials were characterized by Fourier Transform Infrared Spectroscopy (FTIR), Scanning Electron Microscopy (SEM), Energy Dispersive X-Ray Spectroscopy (EDS) and Nitrogen Adsorption Isotherms. Adsorption experimental data were analysed using Langmuir, Freundlich, Dubinin–Radushkevich, Temkin, Redlich–Peterson, Sips and Toth isotherm models along with the evaluation of adsorption energy and standard free energy (ΔG°). The adsorption was observed to be pH dependent. The main mechanism of metal adsorption was found to be a spontaneous charge associated interaction. Electron Spin Resonance (ESR) spectroscopy confirmed that Cr(VI) adsorption was an adsorption-coupled reaction and the adsorbed specie was Cr(V). The hybrid matrix probed its adsorption capacity of Cr(III) in a non-treated tannery wastewater.

1. Introduction

Around the globe industrial activity is the main anthropogenic source of water pollution. The development of cost-effective alternatives to traditional water treatment techniques has gained interest in the last decades since they are more plausible to be applied [1]. Low-cost materials with adsorption capacity for inorganic and organic pollutants are advantageous alternatives to traditional processes, such as membrane filtration, ion exchange or reverse osmosis [2]. Among them, biosorbents are generally considered low-cost since they are used with little or none processing and usually are abundant industrial by-products or waste materials [3]. Examples of low-cost biosorbents are: grainless stalk of corn, cypress cones, seaweeds, dead biomass and polysaccharides such as modified celluloses, chitin and chitosan [4–8].

Natural polyphenols have also been studied in water treatment as flocculant agents and as biosorbents for heavy metal and dyes [9–12]. Polyphenols, such as vegetable tannins, are high molecular weight compounds that occur in almost every part of the higher plants [10]. They cannot be considered as an isolated group of compounds since they present different chemical structures. Among them condensed tannins have flavanoid units that consist predominantly in phloroglucinolic, resorcinolic or pyrogallolic A-rings and catecholic or pyrogallolic B-rings (Supplementary data 1). The interest in developing polyphenol biosorbents relay on the ubiquity of these compounds in plant material which can be easily obtained by solvent extraction from agricultural activity waste materials.

Polyphenols are sparingly soluble in water and immobilization avoids leaching when used as biosorbents [13]. At the same time immobilization is an advantage since it endows the sorbent mechanical stability and a physical support for batch or column water remediation, which also allows its reuse [14,15]. The immobilization of labile organic molecules or polymers requires reaction conditions which ensure to preserve their chemical properties in the final material. The mild conditions of polymerization of the sol–gel method, such as room temperature operation and no need of extreme pH or caustic catalysts, makes it an ideal strategy for inorganic–organic hybrid material development [16]. Literature describes several approaches for the use of sol–gel technology for biosorbent immobilization, such as chitosan, chitin or humin [17,18].

The aim of this work is to generate a hybrid polyphenol–silicon dioxide material for its use as metal sorbent in liquid media. The residual dust from the milling of Yerba mate (*Ilex paraguariensis*) is a waste material and was chosen as polyphenol source

* Corresponding author at: Cátedra de Química Analítica Instrumental, Facultad de Farmacia y Bioquímica, Universidad de Buenos Aires (UBA), Junín 956, C1113AAD Buenos Aires, Argentina. Tel.: +54 11 49648254; fax: +54 11 49648254.
E-mail addresses: ldiaz@ffyb.uba.ar, guillejcopello@yahoo.com.ar (L.E. Diaz).

0927-7765/$ – see front matter © 2012 Elsevier B.V. All rights reserved.
http://dx.doi.org/10.1016/j.colsurfb.2012.08.015

in this work for the synthesis of a polyphenol–silicon dioxide matrix. The consumption of Yerba mate infusion is the most popular tea-like beverage in South America [19]. The Yerba mate residual dust production is associated to Yerba mate production which is about 280000 tons per year in Argentina [20]. The hybrid materials were obtained by the sol–gel method using tetraethoxysilane (TEOS) as the SiO_2 precursor and polyphenols were cross-linked with glutaraldehyde. Pb(II), Cr(III) and Cr(VI) were chosen as model metals for adsorption. Conditions regarding batch optimum pHs, interaction times, and adsorption capacities were studied. Langmuir, Freundlich, Dubinin–Radushkevich, Temkin, Redlich–Peterson, Sips and Toth isotherm models were analysed together with the evaluation of adsorption energy and standard free energy (ΔG°). The hybrid matrix was assayed against a Cr(III) containing tannery wastewater as a suitable tailored remediation biosorbent.

2. Materials and methods

2.1. Reagents and materials

Tetraethoxysilane (TEOS) was purchased from Fluka (Buchs, Switzerland). Glutaraldehyde (25%) and nitric acid (70%) were from J.T. Baker (Phillipsburg, NJ, USA). Folin–Ciocalteau's phenol reagent was acquired from Merck (Darmstadt, Germany). Chromium chloride and Gallic acid were from Riedel-de Haën (Seelze, Germany). Lead nitrate was purchased from Mallinckrodt (USA). Potassium dichromate was from Anedra (Buenos Aires, Argentina). All metal working solutions were made by dilution of the stock solution and concentration verified against the appropriate dilution of Titrisol Lead or Chromium Standards 1000 mg/L (Merck). All other reagents were of analytical grade.

Yerba mate dust (*I. paraguariensis*) as the waste of Yerba mate leaves production was recollected and kindly donated by a Yerba mate producer mill at the province of Misiones, Argentina. Tannery wastewater was kindly donated by a local tanning industry and used without further treatment.

2.2. Polyphenol extraction and quantification

The extraction of Yerba mate polyphenols was done by refluxing 75 g of Yerba mate dust in 300 mL of a given organic solvent for 2 h. Three solvents were tested in their capacity for polyphenol extraction: methanol, ethanol and 2-propanol. The organic extract was centrifuged 10 min at 3000 rpm and then the supernatant was dried in a rotary evaporator until a residue was obtained. The polyphenol containing residue was then resuspended in 0.2 mol/L potassium hydrogen phthalate pH 5 using a volume ten times smaller than the volume obtained from the organic extract.

A spectrophotometric quantification of total polyphenols content was done by the Folin–Ciocalteau method [21]. Two milliliters of Na_2CO_3 (2%, w/v) (Anedra, Argentina) were mixed with 200 μL of the Yerba mate dust organic extract and 200 μL of Folin–Ciocalteau phenol reagent. Samples absorbance was measured at 725 nm in a UV–vis spectrophotometer (Cecil CE 3021, Cambridge, England) after 30 min of incubation. Gallic acid was used as a standard and the total phenolic content was expressed as gallic acid equivalents (mg of gallic acid/mL Yerba mate dust extract).

2.3. SiO_2–polyphenol matrix synthesis

Two types of matrices were synthesized: (1) blank matrices containing a SiO_2 polymeric network (named SiO_2) and (2) SiO_2–polyphenol containing matrices (named Si–Pol). For the synthesis of both matrices, a TEOS sol was prepared by sonicating (35 kHz, Transsonic Tl-H-5, Elma, Germany) a mixture of 10 mL TEOS, 0.6 mL of 0.05 mol/L HCl and 2 mL of water for 30 min at 25 °C. For Si–Pol matrix synthesis equal amounts of TEOS sol and the phthalate resuspended Yerba mate extract were mixed. For SiO_2 blank matrices phthalate buffer was use instead of the polyphenol–phthalate solution. Polymerization took place at 25 °C within 10 min. The matrix was aged during a week at 4 °C and a relative humidity of no less than 90%.

An amount of 0.6 g of each matrix, SiO_2 or Si–Pol, were then incubated 16 h at 25 °C in 1.5 mL of 0.5 mol/L K_2HPO_4 pH 7.4 containing variable amounts of glutaraldehyde. The crosslinking efficiency was evaluated in a range from 0.01 to 5% glutaraldehyde. Finally, the matrices were washed three times in distilled water during 2 h and stored at 4 °C until use.

2.4. Characterization

FTIR transmission spectra were acquired in the range of 4000–450 cm^{-1} using a Fourier Transform Infrared Spectrometer (FTIR) (Perkin Elmer, Spectrum One IR). All samples were previously dried for 24 h under vacuum to avoid water related bands interference. Samples were analysed using a Zeiss Supra 40 microscope for Scanning Electron Microscopy (SEM), while elemental analyses were carried out using an Energy Dispersive Analyser (EDS) (Oxford Instruments). Before performing the N_2 gas adsorption–desorption isotherms, all samples were degassed for 24 h at 50 °C under high vacuum. N_2 adsorption and desorption isotherms were performed in duplicate at 77.7 K employing N_2 spectroscopic grade. The specific surface area (S_{BET}) and total pore volume (TPV) were estimated by the Brunauer–Emmett–Teller (BET) and Barrett–Joyner–Halenda (BJH) methods, respectively. Matrices water content was determined with a moisture analyser at constant temperature (105 °C) (MX-50, A&D Company, Tokyo, Japan).

2.5. ESR measurements

The Si–Pol matrices were placed in a quartz tube and Electron Spin Resonance (ESR) spectra were recorded at 20 °C in an X-band ESR Spectrometer Bruker EMX plus (Bruker Instruments, Inc., Berlin, Germany). The spectrometer settings were: sweep width 1400.00 G; microwave power 10.0 mW; modulation amplitude 0.5 G and conversion time 5.12 ms. For g factor calculation, Diphenylpicrylhydrazyl (DPPH, Aldrich) ($g = 2.0036$) was used as an internal standard.

2.6. Adsorption experiments

Adsorption experiments were carried out by a batch method at room temperature (25 °C) with constant stirring (120 rpm). A weighted mass of SiO_2 or Si–Pol matrices (0.4 g) was added to an aqueous solution (5 mL) of Pb(II), Cr(III) or Cr(VI), ranging from 0.01 to 200 mg/L. The effect of the amount of crosslinking agent, media pH, interaction times and adsorption isotherms were determined by metal decay in the solution supernatant. For the analysis of the adsorption isotherms, in order to evaluate the mass of metal adsorbed in the Si–Pol matrices, microwave digestion of the matrices (MLS 1200 Mega, Milestone, Bergamo, Italy) was carried out in a HNO_3:H_2O_2 mixture (9:1) prior to Electrothermal Atomic Absorption Spectroscopy (ETAAS) determination. Lead and Chromium determinations were done with a Buck Scientific VGP 210 Atomic Absorption Spectrophotometer (E. Norwalk, CT, USA) by the electrothermal atomization method using pyrolytic graphite tubes. Nickel nitrate 0.1% was used as matrix modifier in lead determination.

Si–Pol matrices were tested against a real sample: tannery wastewater was assayed for Cr(III) adsorption without treatment.

Two conditions were tested; one without dilution and one diluted ten times.

All adsorption assays were carried out in plastic vessels. Blank experiments were conducted in order to verify the absence of metal precipitation and/or metal adsorption to the walls of the vessels. All experiments and their corresponding measurements were conducted in triplicate under identical conditions and statistically analysed by one-way ANOVA and by Bonferroni Multiple comparison post-test if ANOVA $p < 0.05$. R language and environment was used for statistical computing and graphics [22].

3. Results and discussion

3.1. Polyphenol extraction and the influence of cross-linking agent concentration

The total polyphenol content of the ethanol and methanol extracts was found to be not significantly different, being 31 ± 2 mg of gallic acid/mL and 31 ± 6 mg of gallic acid/mL, respectively. On the other hand, the use of 2-propanol lead to lower polyphenol contents in the extracts (12 ± 3 mg of gallic acid/mL). This encourages the use of ethanol, a more environmentally friendly solvent.

When non-cross-linked Si–Pol matrices were immersed in an aqueous media, polyphenols eluted from the SiO_2 matrix and no metal adsorption was observed. Therefore glutaraldehyde cross-linking was evaluated in order to retain polyphenols in the matrix. The influence of the glutaraldehyde concentration used as cross-linker was evaluated in its effect on Pb(II) adsorption percentage (Supplementary data 2). Lead adsorption showed to be in all cases higher for the Si–Pol matrices than for the SiO_2 matrices (significantly different, $p < 0.01$). Among the Si–Pol matrices the higher adsorption percentage was obtained by the ones cross-linked with 0.1% glutaraldehyde. Below 0.1% the amount of glutaraldehyde was not enough to ensure that all polyphenols were completely cross-linked and a percentage was eluted during the washing steps with the consequent decrease in adsorption. Above 0.1% glutaraldehyde, it was also observed a drop in adsorption. The decrease in the amount of the adsorption active sites was probably due to: (a) a depletion of adsorption sites by steric impediment, and/or (b) an excessive cross-linking involving *o*-dihydroxyphenyl metal quelating groups. Therefore 0.1% glutaraldehyde was used in all further experiments.

3.2. Matrix characterization

As can be seen in SEM images of SiO_2 and Si–Pol matrices, topography of the two matrices is clearly different (Supplementary data 3). When SiO_2 matrix seems to have few pores over its surface, Si–Pol matrix image shows larger pores of a highly porous material. This is consistent with the nitrogen sorption isotherms results (Supplementary data 4 and 5). It could be seen an isotherm I type behaviour for SiO_2 matrix which is present in some non-porous or microporous materials. On the other hand, an isotherm type IV behaviour could be evidenced for Si–Pol matrix where it could also be observed the typical hysteresis loop of mesoporous materials [23]. It is well known that the immobilization of organic molecules or polymers can influence the condensation process of SiO_2 leading to materials with different topography and porosity which explains the differences observed in the SEM images and BET results [24]. However, the presence of polyphenols within the SiO_2 network did not show to have a strong effect on matrix water content (Supplementary data 4) probably due to ageing and storage conditions (90% relative humidity at 4 °C).

EDS spectroscopy was used to confirm the presence of the polyphenols in the matrices. Only in the EDS spectrum of the Si–Pol matrix the peak corresponding to carbon atoms could be evidenced (Supplementary data 6). The immobilized polyphenols would be the main source of this signal since C atoms from glutaraldehyde are not detected in the cross-linked SiO_2 spectrum, probably because its low proportion compared with other matrix components. The silicon and oxygen atom peaks are present in both matrices spectra, confirming the presence of the silicon oxide network.

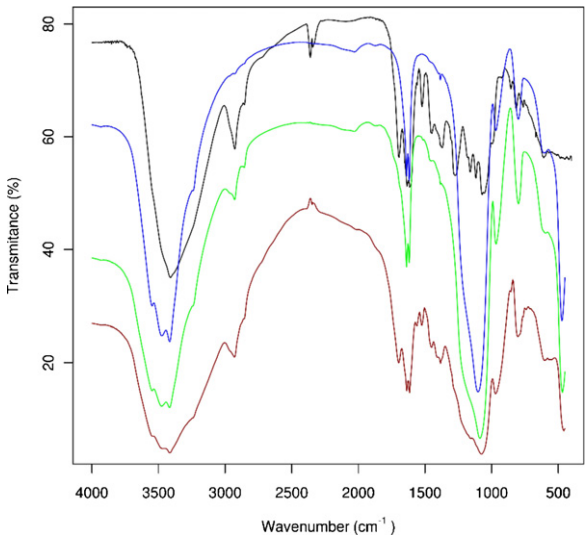

Fig. 1. FTIR spectra of the (a) polyphenol extract, (b) the SiO_2 matrix, (c) the cross-linked Si–Pol and (d) the non-cross-linked Si–Pol matrices.

IR spectra of the SiO_2 matrix, the polyphenol extract, the cross-linked Si–Pol and the non-cross-linked Si–Pol matrices are shown in Fig. 1. As expected, the presence of the silicon oxide network is detected in all matrices spectra except in the polyphenol extract spectrum. This presence is evidenced by the characteristic silicon oxide bands at 790 cm^{-1}, 970 cm^{-1} and 1080 cm^{-1} corresponding to symmetric Si—O—Si bond stretching, Si—OH bond stretching and asymmetric Si—O—Si bond stretching respectively [25,26]. Almost all the organic group related bands that appear in the polyphenol extract spectrum and had not been blocked by the intense SiO_2 bands, also appear in the cross-linked Si–Pol and the non-cross-linked Si–Pol matrices spectra. This is not the case for the 1694 cm^{-1} band which is absent in the cross-linked Si–Pol spectrum. These band accounts for C=O stretching of conjugated carbonyl groups, such as quinonic compounds or phenols capable of tautomeric equilibrium [27]. This suggests that glutaraldehyde is cross-linking the polyphenols by anchoring to these groups. Plant polyphenols, like tannins are reactive with carbonyl containing compounds due to the strong nucleophilicity of their A-rings, maintaining its metal adsorption capacity by means of ortho-hydroxyl groups in the B-ring [11]. As mentioned above, the non-cross-linked Si–Pol matrices showed that the solely SiO_2 network is not capable to retain polyphenols within the matrix, which suggest that there is no covalent bonding between SiO_2 and polyphenols under this conditions. Thus, the obtained material would be an interpenetrated hybrid material composed of a SiO_2 network and a polyphenol–glutaraldehyde polymer.

3.3. Effect of pH on adsorption behaviour

The effect of media pH on metal adsorption behaviour was analysed in the pH range 3–7 (Table 1). For the cases of Pb^{2+} and Cr^{3+}, the higher differences between Si–Pol and SiO_2 matrices adsorption percentage were seen at pH 3. This difference decreases as pH increases. This is probably due to a decrease in polyphenol related adsorption and an increase in SiO_2 network related adsorption [14].

Table 1
Effect of pH on adsorption behavior.

Metal	Matrix	Adsorption (%)				
		pH				
		3	4	5	6	7
Pb(II)	SiO_2	13.5 ± 0.6	30.3 ± 0.1	9 ± 2	21 ± 4	N.T.[a]
	Si–Pol	55 ± 4	38 ± 2	17 ± 3	49 ± 5	N.T.
Cr(III)	SiO_2	34.7 ± 0.6	7 ± 2	27 ± 4	20 ± 8	N.T.
	Si–Pol	64 ± 1	4 ± 2	64 ± 6	57 ± 2	N.T.
Cr(VI)	SiO_2	11 ± 2	10.1 ± 0.9	8 ± 1	6 ± 1	5 ± 1
	Si–Pol	54 ± 7	35 ± 4	29.4 ± 0.7	20 ± 4	10.6 ± 0.8

[a] Not tested due to metal precipitation.

In a previous study, it was demonstrated that polyphenol related adsorption on Yerba mate leaves is higher at low pHs where cations form insoluble complexes with polyphenol's *o*-dihydroxyphenyl groups [28]. In all cases the higher adsorption of the Si–Pol matrices was observed at pH 3 (significantly different, $p < 0.05$), except for the case of Cr(III) adsorption where the adsorption related to the SiO_2 network is added to polyphenols quelating activity. As a consequence, Cr(III) adsorption at pH 6 was almost the same than at pH 3 (no significantly different).

On the other hand, Cr(VI) adsorption decreased with pH increase but no rise in SiO_2 matrix related adsorption was observed. This is probably due to electrostatic repulsion between chromate anions and the negative charge density of the surface of the SiO_2 network above its point of zero charge (around pH 2) [29].

Other researchers have proposed that the biosorption of Cr(VI) is carried out by an adsorption-coupled reduction process [6,30]. Cr(VI) would be reduced to Cr(III) in acidic conditions by organic compounds from the biosorbent. Then, as described above, the adsorption of Cr(III) is promoted at acidic pH. ESR spectroscopy was used to verify the Cr(VI) reduction followed by Cr(III) adsorption on Si–Pol matrices. The ESR spectra of Cr(VI) interacting with the matrices were obtained at 1 h and 48 h incubation times (Fig. 2). Being Cr(VI) non-paramagnetic, therefore ESR negative, it was expected that at short incubation times no signals would be observed in the spectrum. Also, if an adsorption-coupled reduction process is taking place, at larger incubation times the signal of the paramagnetic Cr(III) should be observed. The first

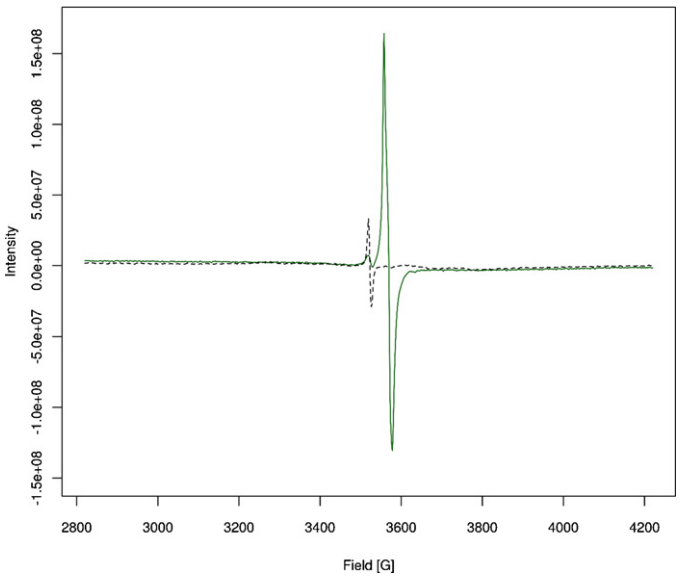

Fig. 2. EPR spectra of Si–Pol matrices incubated with 10 mg/L Cr(VI) for 1 h (a) and 48 h (b).

assumption is evidenced in the 1 h incubation spectrum where only a semiquinone radical signal is observed [31]. On the other hand, for the 48 h incubation spectrum it can be seen the signal of the paramagnetic Cr(V) (g_{iso} = 1.9798). This behaviour could be explained by a deficient electron supply for the reduction of Cr(VI) to Cr(III) and the capability of the polyphenols to stabilize Cr(V) by multiple hydroxy and carboxy group coordinations, already described by other researchers for polyhydroxylic and polycarboxylic compounds [32,33]. Therefore, although an adsorption-coupled reduction is taking place in Cr(VI) adsorption, the cationic Cr(V) would be the specie adsorbed by the matrix instead of Cr(III).

3.4. Adsorption kinetics

Adsorption kinetic experimental results are shown in Fig. 3. These plots show adsorbed metal over time at pH 3. In order to analyse the metals uptake rates kinetic analysis using the pseudo-first-order, pseudo-second-order, Elovich and the modified Freundlich equations were performed in their non-linear forms. Pseudo-1st order and pseudo-2nd order are described by [13,34]:

$$q_t = q_{eq}(1 - e^{-k_1 \cdot t}) \quad (1)$$

$$q_t = \frac{q_{eq}^2 \cdot k_2 \cdot t}{1 + (q_{eq} \cdot k_2 \cdot t)} \quad (2)$$

where q_t and q_{eq} are adsorption capacities at time t (h) and at equilibrium respectively (mg/g), k_1 (h^{-1}) and k_2 (g/(mg h)) are the sorption rate constants for the pseudo-1st and pseudo-2nd order models, respectively. The initial sorption rate h_0 (mg/(g h)) for the pseudo-2nd order kinetic model was written as: $h_0 = q_{eq}{}^2 k_2$.

Considering $q_t = q_t$ at $t = t$ and $q_t = 0$ at $t = 0$, the Elovich rate equation becomes [35]:

$$q_1 = \frac{1}{\beta} \ln(1 + (\alpha \cdot \beta \cdot t)) \quad (3)$$

where constant α (mg/(g h)) is the initial adsorption rate and β (g/mg) is related to the extent of surface coverage and the activation energy involved in chemisorption processes [36]. This equation assumes that the active sites of the sorbent are heterogeneous in nature and therefore exhibit different activation energies for chemisorption [35].

The modified Freundlich model was originally developed by Kuo and Lotse [37]:

$$q_t = k_F \cdot C_0 \cdot t^{1/m} \quad (4)$$

where k_F (L/(mg h)) is the apparent adsorption rate constant, C_0 (mg/L) the initial sorbate concentration and m (dimensionless) is the Kuo–Lotse constant [37]. This model can describe surface diffusion-controlled processes. Particularly, it can describe kinetics controlled by intra-particle diffusion when m approaches a value of 2 [13]. The modelled kinetic parameters are summarized in Table 2.

In previous papers non-linear model's goodness-of-fit was evaluated by means of the coefficient of determination (R^2). Recent works propose more appropriate ways to compare models by different selection criteria [38]. The adequacy of the models in this work was compared using Akaike's information criteria (AIC) according to the formula [39]:

$$\text{AIC} = -2 \log\text{-likelihood} + km \quad (5)$$

where m represents the number of parameters in the fitted model and $k = 2$ for the usual AIC. The preferred model is the one with the lowest AIC value. When n (number of observations) is small, the second-order corrected AIC value (AICc) becomes accurate [38,40]:

$$\text{AICc} = \text{AIC} + \frac{2(m+1)(m+2)}{n-m-2} \quad (6)$$

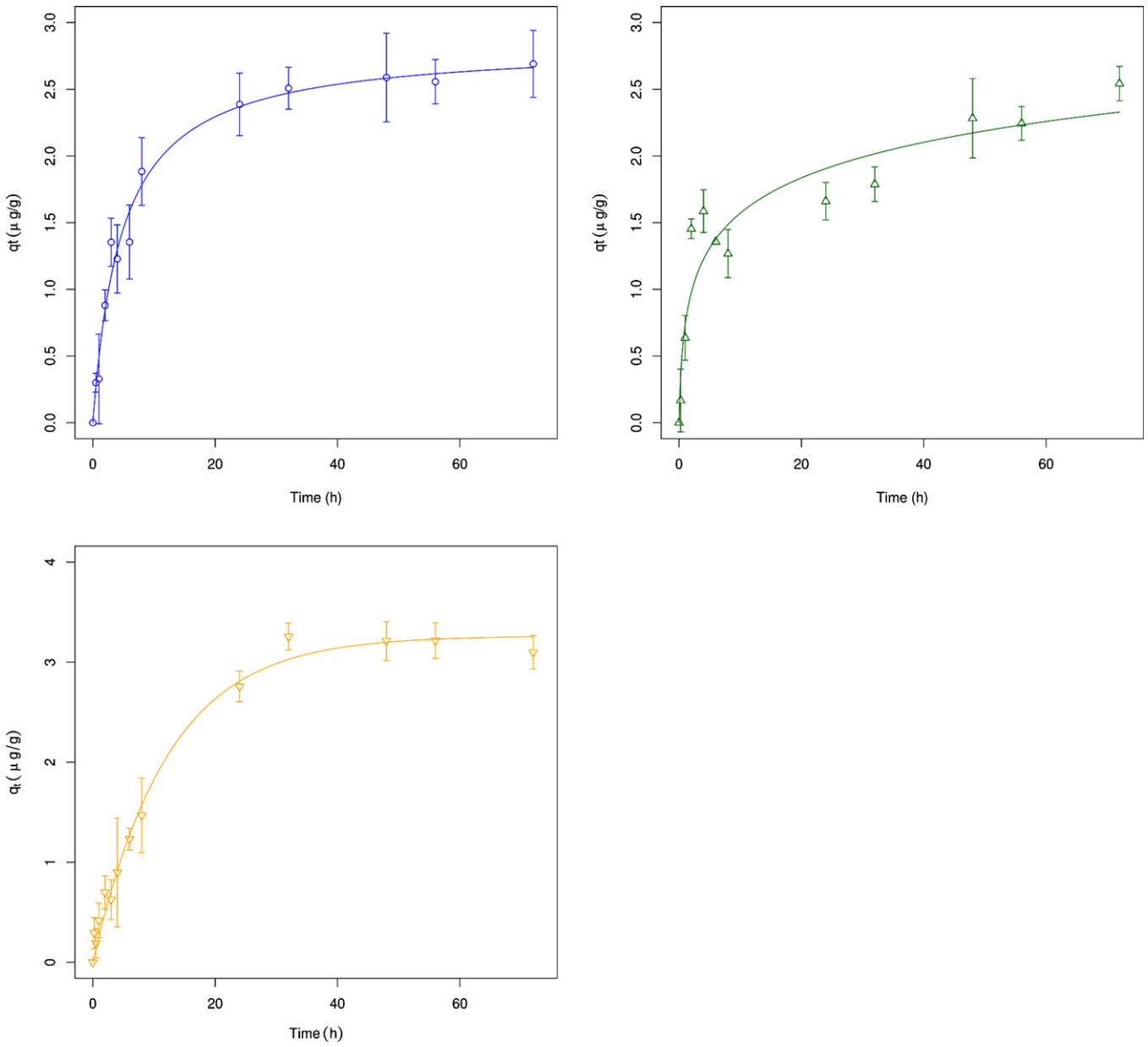

Fig. 3. Metal adsorption over time at pH 3 for Pb(II) (a), Cr(III) (b) and Cr(VI) (c). Pseudo-second order plot is presented for Pb(II), Elovich plot is presented for Cr(III) and pseudo-first order plot is presented for Cr(VI).

As supplementary model selection criteria the Evidence Ratio of Akaike weights (w_i(AIC)), the residual-sum-of-squares (RSS) and the root-mean-square-errors (RMSE) were analysed according to [38,41]:

$$w_i(\mathrm{AIC}) = \frac{e^{(-0.5.\Delta_i(\mathrm{AIC}))}}{\sum_{k=1}^{K} e^{(-0.5.\Delta_i(\mathrm{AIC}))}} \quad (7)$$

$$\mathrm{RMSE} = \sqrt{\frac{1}{n-2}\sum_{i=1}^{n}(q_{\mathrm{exp}} - q_{\mathrm{cal}})^2} \quad (8)$$

$$\mathrm{RSS} = \sum_{i=1}^{n} w_i (q_{\mathrm{exp}} - q_{\mathrm{cal}})^2 \quad (9)$$

where the Evidence Ratio (Er) is obtained by the quotient of the weights of lowest AIC model and the model to be compared. Thus, Er indicates how many times the lowest AIC model fits better than the other one [41]. The subscripts "*exp*" and "*calc*" show the experimental and calculated values. Smaller RMSE and RSS values represent better curve fittings [38].

Literature shows that in most cases of biosorption pseudo-2nd order equation fit better for the whole range of contact times than the pseudo-1st order. This is evidenced in Pb(II) adsorption kinetics which showed better agreement for the pseudo-2nd order model, followed by Elovich model. A good adjustment to the pseudo-2nd order model would indicate that chemisorption is the rate limiting step [42]. Other researchers have reported that Elovich model have suitable agreement for chemisorption processes on heterogeneous sites of biosorbents [35]. This was the case of Cr(III) sorption which fitted better to Elovich model, followed by the modified Freundlich model. The value of the *m* parameter of the last model, which is far from 2, suggests that the intra-particle diffusion in the pores of the sorbent is negligible [43]. On the other hand, Cr(VI) fitted better to the pseudo-1st order model followed by pseudo-2nd order model. Thus, considering the proposed adsorption-coupled reduction

Table 2
Kinetic parameters for metal adsorption by the Si–Pol matrices.

Model	Parameter	Pb(II)		Cr(III)		Cr(VI)	
		Value	GOF[a]	Value	GOF	Value	GOF
Pseudo 1st order	q_{eq} (μg/g)	2.54 ± 0.08	AICc = 35 Er = 5.4	2.02 ± 0.08	AICc = 34 Er = 85411	3.26 ± 0.08	AICc = 6 Er = 1.0
	k_1 (h^{-1})	0.17 ± 0.02	RMSE = 0.324 RSS = 5.13	0.33 ± 0.07	RMSE = 0.359 RSS = 4.37	0.082 ± 0.006	RMSE = 0.241 RSS = 2.80
Pseudo 2nd order	q_{eq} (μg/g)	2.8 ± 0.1	AICc = 32 Er = 1.0	2.21 ± 0.09	AICc = 23 Er = 396	4.0 ± 0.1	AICc = 13 Er = 24
	k_2 (g/(μg h))	0.07 ± 0.01	RMSE = 0.313 RSS = 4.79	0.18 ± 0.05	RMSE = 0.306 RSS = 3.19	0.020 ± 0.003	RMSE = 0.258 RSS = 3.19
Elovich	α (μg/(g h))	1.1 ± 0.3	AICc = 38 Er = 19.3	2.2 ± 0.8	AICc = 11 Er = 1.0	0.44 ± 0.06	AICc = 22 Er = 3274
	β (g/μg)	1.7 ± 0.2	RMSE = 0.332 RSS = 5.40	2.6 ± 0.2	RMSE = 0.257 RSS = 2.24	0.96 ± 0.07	RMSE = 0.286 RSS = 3.92
Modified Freundlich	k_F (L/(μg h))	1.3 ± 0.1	AICc = 51 Er = 16470	0.98 ± 0.09	AICc = 12 Er = 1.5	0.67 ± 0.07	AICc = 39 Er = 14646972
	m	3.2 ± 0.3	RMSE = 0.381 RSS = 7.11	3.7 ± 0.4	RMSE = 0.260 RSS = 2.30	2.3 ± 0.1	RMSE = 0.340 RSS = 5.56

[a] GOF, goodness-of-fit.

process for Cr(VI) adsorption, probably reduction would be the rate limiting step of the overall process. From Fig. 3 it could be observed that in all cases chemical equilibrium is achieved after 24 h incubation time. Therefore, all further experiments were carried out with 24 h incubation time.

3.5. Adsorption isotherms

In this work adsorption isotherms are represented by a q_{eq} *vs* C_{eq} plot, where C_{eq} is the metal concentration in the incubation solution (mg/L) at equilibrium and q_{eq} is the adsorption capacity,

Table 3
Isotherm model parameters for Pb(II), Cr(III) and Cr(VI) adsorption by the Si–Pol matrices.

Model	Parameter	Pb(II)		Cr(III)		Cr(VI)	
		Value	GOF[a]	Value	GOF	Value	GOF
Langmuir	q_m (mg/g)	1.78 ± 0.08	AICc = −103 RSS = 0.289	2.7 ± 0.1	AICc = −51 RSS = 0.558	4.5 ± 0.1	AICc = −18 RSS = 1.176
	K_a (L/mg)	0.026 ± 0.003	Er = 1.0 RMSE = 0.078	0.021 ± 0.002	Er = 2×10^{11} RMSE = 0.118	0.033 ± 0.003	Er = 5×10^{8} RMSE = 0.176
	ΔG° (kJ/mol)	−21.3 ± 0.4		−17.23 ± 0.06		−18.47 ± 0.04	
Freundlich	k	0.12 ± 0.01	AICc = −75 RSS = 0.513	0.179 ± 0.009	AICc = −103 RSS = 0.154	0.47 ± 0.03	AICc = −22 RSS = 1.058
	n	0.53 ± 0.03	Er = 0.9 RMSE = 0.103	0.50 ± 0.01	Er = 1.0 RMSE = 0.062	0.42 ± 0.01	Er = 8×10^{7} RMSE = 0.167
Temkin	α_T (L/mg)	1.7 ± 0.4	AICc = −9 RSS = 2.025	5 ± 1	AICc = 22 RSS = 3.447	8 ± 2	AICc = 64 RSS = 10.02
	B (kJ/mol)	12.1 ± 0.9	Er = 2×10^{20} RMSE = 0.205	10.8 ± 0.8	Er = 1×10^{27} RMSE = 0.293	5.6 ± 0.4	Er = 3×10^{26} RMSE = 0.513
D–R	q_{DR} (mg/g)	12 ± 1	AICc = −85 RSS = 0.422	13.8 ± 0.8	AICc = −97 RSS = 0.178	18.4 ± 0.9	AICc = −49 RSS = 0.523
	K_{DR} ($mol^2/(kJ^2)$)	0.0042 ± 0.0002	Er = 9187 RMSE = 0.094	0.0039 ± 0.0001	Er = 18 RMSE = 0.067	0.0033 ± 0.0001	Er = 116 RMSE = 0.117
	E_{DR} (kJ/mol)	11.0 ± 0.3		11.3 ± 0.2		12.4 ± 0.2	
R–P	K_{RP} (L/mg)	0.047 ± 0.007	AICc = −101 RSS = 0.289	0.18 ± 0.06	AICc = −89 RSS = 0.201	0.5 ± 0.1	AICc = −58 RSS = 0.383
	α_{RP} ($(L/mg)^{n_{RP}}$)	0.03 ± 0.02	Er = 3.1 RMSE = 0.077	0.5 ± 0.3	Er = 731 RMSE = 0.071	0.5 ± 0.2	Er = 1.0 RMSE = 0.100
	n_{RP}	1.0 ± 0.1		0.63 ± 0.05		0.70 ± 0.02	
Sips	q_{mS} (mg/g)	1.6 ± 0.1	AICc = −102 RSS = 0.282	2.8 ± 0.4	AICc = −57 RSS = 0.444	5.0 ± 0.4	AICc = −34 RSS = 0.698
	K_S (L/mg)	0.033 ± 0.005	Er = 1.8 RMSE = 0.077	0.019 ± 0.007	Er = 5×10^{9} RMSE = 0.105	0.025 ± 0.005	Er = 9×10^{4} RMSE = 0.135
	n_S	1.1 ± 0.1		0.8 ± 0.1		0.79 ± 0.06	
Toth	q_{mT} (mg/g)	1.7 ± 0.2	AICc = −101 RSS = 0.287	2.8 ± 0.6	AICc = −53 RSS = 0.499	6.0 ± 0.9	AICc = −41 RSS = 0.604
	b_T (L/mg)	0.026 ± 0.003	Er = 2.8 RMSE = 0.077	0.027 ± 0.004	Er = 5×10^{10} RMSE = 0.112	0.05 ± 0.01	Er = 5950 RMSE = 0.126
	n_T	1.1 ± 0.3		0.8 ± 0.3		0.5 ± 0.1	

[a] GOF, goodness-of-fit.

expressed as the mass of adsorbed metal per mass unit of sorbent (mg/g) determined by mineralization of the Si–Pol matrices. Two and three parameters isotherm models were analysed in order to achieve a better understanding of the adsorption process.

3.5.1. Two parameters adsorption isotherms

Langmuir model was developed on the assumption that a single specie of the sorbate will adsorb on the sorbent in a monolayer to homogeneous adsorption sites while Freundlich presents a better experimental adjustment to materials with heterogeneous adsorption sites and interactions [34]. Langmuir and Freundlich adsorption isotherms can be expressed using Eqs. (10) and (11) respectively [44]:

$$q_{eq} = \frac{q_m \cdot K_a \cdot C_{eq}}{1 + K_a \cdot C_{eq}} \tag{10}$$

$$q_{eq} = k \cdot C_{eq}^{n} \tag{11}$$

where K_a is the adsorption equilibrium constant (L/mg), q_m is the maximum adsorption capacity (mg/g) and k and n are arbitrary parameters. The dimension of k depends on the value of n.

The Temkin isotherm is represented by the following equation [8]:

$$q_{eq} = \frac{RT}{B} \ln(\alpha_T \cdot C_{eq}) \tag{12}$$

where constant B (kJ/mol) is the variation of adsorption energy, R is the universal gas constant (kJ/(mol K)), T is the temperature (K) and α_T is the equilibrium binding constant (L/mg) corresponding to the maximum binding energy. The Temkin isotherm assumes that the heat of adsorption of all the molecules in a layer decreases linearly due to adsorbent–adsorbate interactions. Also, a positive variation of adsorption energy implies an exothermic reaction [38].

The Dubinin–Radushkevich (D–R) Eq. (13) was originally developed for the adsorption of vapours by microporous solids and has been studied for its application in the adsorbate–adsorbent interaction in liquid solutions. For liquid–solid phase adsorption the amount adsorbed corresponding to any adsorbate concentration is assumed to be a Gaussian function of the Polanyi potential (ε) [45,46]:

$$q_{eq} = q_{DR} e^{-K_{DR}\varepsilon^2} \tag{13}$$

with

$$\varepsilon = RT \ln\left(1 + \frac{1}{C_{eq}}\right) \tag{14}$$

where q_{DR} is the maximum adsorption capacity (mg/g), K_{DR} is a constant related to sorption energy (mol^2/(kJ^2)).

3.5.2. Three parameters adsorption isotherms

The Redlich–Peterson (R–P) model is a three-parameter extended form of the Langmuir model and can be expressed as [47]:

$$q_{eq} = \frac{K_{RP} \cdot C_{eq}}{1 + \alpha_{RP} \cdot C_{eq}^{n_{RP}}} \tag{15}$$

where K_{RP} (L/mg) and α_{RP} ((L/mg)$^{n_{RP}}$) are the R–P constants. The n_{RP} parameter (dimensionless) represents the heterogeneity of the binding surface. If n_{RP} tends to 1 R–P model results in Langmuir model. When n_{RP} tends to 0 R–P model depicts Henry law. In order to obey the constraints used during derivation of R–P model n_{RP} should be subjected to the constraints $0 < n_{RP} < 1$ [47].

The Sips model combines Langmuir and Freundlich models and is described by [47]:

$$q_{eq} = \frac{q_{mS} \cdot (K_S \cdot C_{eq})^{nS}}{1 + (K_S \cdot C_{eq})^{ns}} \tag{16}$$

where q_{mS} (mg/g) and K_S (L/mg) are the maximum adsorption capacity and the adsorption equilibrium constant, respectively. The n_s parameter represents system heterogeneity as in R–P model. Also, when n_s is close to 1, Sips model resembles Langmuir model.

The Toth model is derived applying the potential theory for the sorption of sorbate molecules onto surface containing sorption sites of heterogeneous nature and is represented by the following equation [47]:

$$q_{eq} = \frac{q_{mT} \cdot b_T \cdot C_{eq}}{(1 + (b_T.C_{eq})^{n_T})^{1/n_T}} \tag{17}$$

where q_{mT} (mg/g) and b_T (L/mg) are the maximum adsorption capacity and the adsorption equilibrium constant, respectively. The n_T parameter (dimensionless) represents the heterogeneity of the adsorption process. If $n_T = 1$ Toth models represents the Langmuir equation, which is consistent with a homogeneous sorption behaviour. The values $n_T < 1$ relate to heterogeneous surfaces where the sorbate–adsorbent interactions are greater than those between the adsorbed molecules. The values $n_T > 1$ relate to the reverse situation [48].

The adsorption isotherms are shown in Fig. 4, where the best fit model is represented. Parameters obtained for the non-linear regression of isotherm adsorption models are summarized in Table 3. Except for Pb(II) adsorption, experimental data showed better agreement for models that describe adsorption to heterogeneous surfaces. This behaviour was expected since Yerba mate contains a wide variety of polyphenols, therefore, multiple adsorption sites [19]. Cr(III) adsorption data fitted better to Freundlich model and Cr(VI) adsorption data to R–P model. In both cases the heterogeneity parameter values of R–P, Sips and Toth models were below the unity, which is consistent with a heterogeneous sorbate–adsorbent interaction. Nevertheless, the value of Toth and Sips maximum adsorption capacity parameters were close to the Langmuir q_m value. This could be due to a combined effect of the presence of heterogeneous adsorption sites and a tendency of these sites to be saturated at high metal concentrations. On the other hand, the adsorption of Pb(II) in the Si–Pol matrices showed better adjustment to Langmuir model, which suggests a greater homogeneity in the sorbate–adsorbent interaction than for Cr(III) and Cr(VI). Also, the heterogeneity parameter values of R–P, Sips and Toth models were close to the unity, which is consistent with the good adjustment to Langmuir model.

3.6. Evaluation of adsorption energy and standard free energy

If the adsorbent surface is heterogeneous and homogeneous subregions are considered, an average free energy value could be calculated using D–R Eqs. (13) and (18) [49]:

$$E_{DR} = (2K_{DR})^{-1/2} \tag{18}$$

where E_{DR} is the mean free energy of adsorption (kJ/mol). The type of adsorption interaction can be deducted from the value of the mean free energy of adsorption. The standard free energy (ΔG°) of the process is related to the adsorption equilibrium constant (K_a), from Langmuir equation (10), by the following equation [50]:

$$\Delta G^\circ = -RT \ln K_a \tag{19}$$

E_{DR} and ΔG° values are summarized in Table 3. For all metals D–R isotherm model showed good agreement. Specially, in the case of Cr(III) and Cr(VI), in which the goodness-of-fit values indicate that D–R was the 2nd best fitted model. In an adsorption process where charge associated interaction prevails, the magnitude of E_{DR} is in the range of 8–16 kJ/mol [51]. This was the case of Pb(II), Cr(III) and Cr(VI) calculated mean free energy of adsorption, which is consistent with a previous work where metal adsorption was

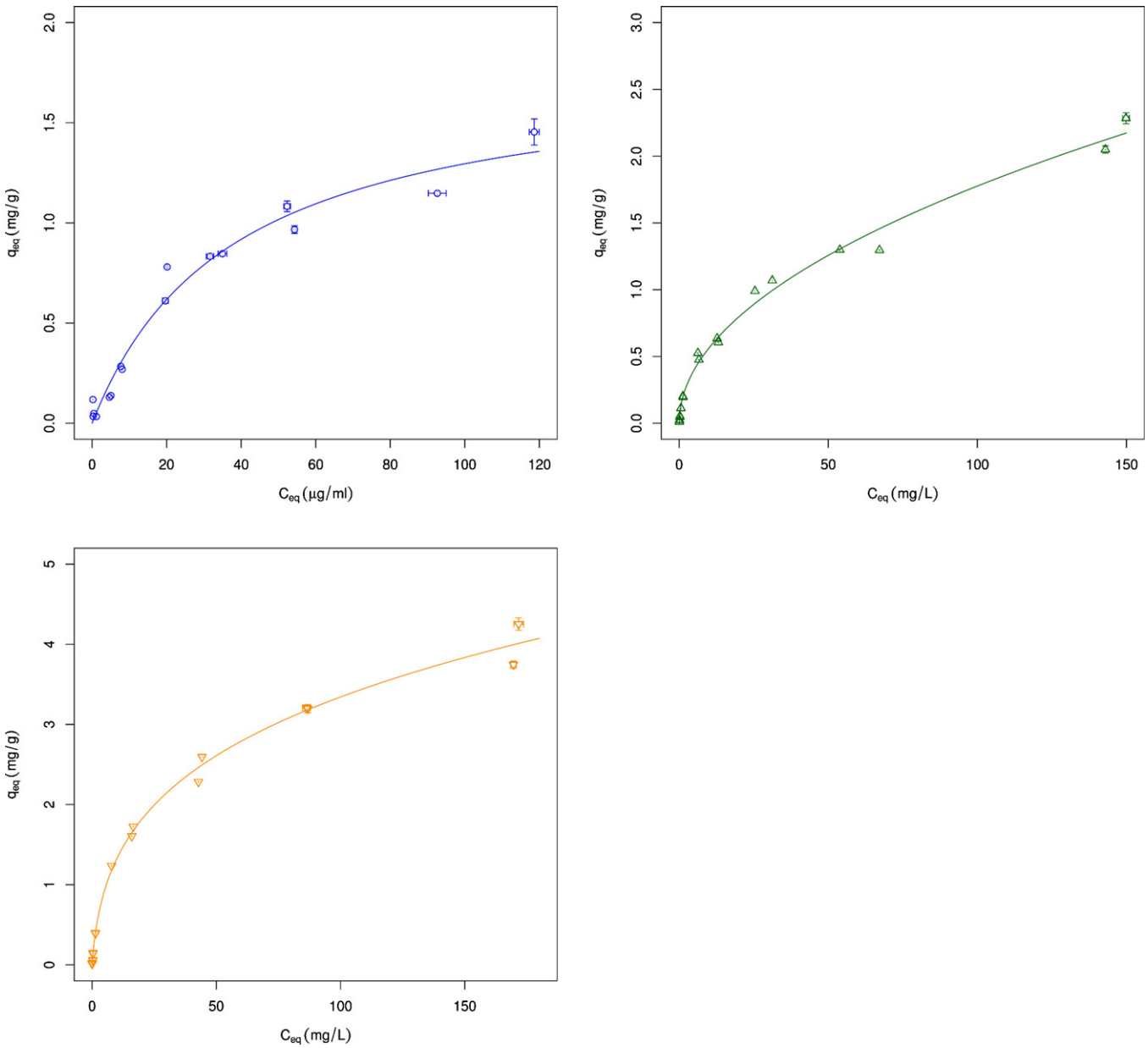

Fig. 4. Adsorption isotherms for Pb(II), Cr(III) and Cr(VI). Langmuir plot is presented for Pb(II), Freundlich plot is presented for Cr(III) and Redlich–Peterson plot is presented for Cr(VI).

studied over exhausted Yerba mate leaves [28]. This type of interaction is explained by the presence of *o*-dihydroxyphenyl metal chelating groups in polyphenolic structures of the Si–Pol matrices [52]. Although the process of Cr(VI) adsorption involves a reduction to Cr(V), the mean free energy of adsorption value also accounts for charge associated interaction. Probably the energetically dominant step of the whole process is the Cr(V) adsorption. The negative values obtained for the standard free energy of all three metal ions tested shows the spontaneity of the process at these conditions.

3.7. Remediation of Cr(III) from a real wastewater sample and recovery of the metals

Taking into account the material adsorption behaviour, it was considered that an acidic tannery wastewater could be the target for the use of the Si–Pol matrices in Cr(III) tailored remediation. Tannery wastewater was found to have a high amount of Cr(III) (4800 mg/L) in a highly acidic media. Since Si–Pol matrices showed to have higher adsorption of metals at low pH, it was considered that their application in tannery wastewater remediation was straightforward. Cr(III) adsorption was found to be 55% in the tenfold diluted tannery wastewater and 13% for the undiluted sample, proving it direct application in this type of sample.

Metal recovery from the matrix was assessed in order to evaluate the possibility of a proper disposal of the pollutant or its recovery for purification. Since polyphenols act as adsorbents at acidic pH and most metal cations precipitate at alkaline media, the metal recovery was assayed at strong acidic-oxidant conditions (wet mineralization). Wet mineralization allowed to recover nearly 100% of the adsorbed metals (Pb(II), Cr(III) and Cr(VI)) but leads to the polyphenol decomposition, ending the material's quelating activity. On the other hand, the SiO_2 structure of the Si–Pol matrices remains stable. In this way the product of the mineralization consist of a acid liquid supernatant containing the pollutant metals and a solid SiO_2 residue.

4. Conclusion

A low-cost biosorbent-hybrid material ready for application was obtained in this work. Yerba mate residual dust was used as a polyphenol source and the organic extract was immobilized within a SiO_2 matrix to form an interpenetrated polymer after glutaraldehyde cross-linking. Characterization results suggest that glutaraldehyde is cross-linking polyphenols by ketone residues. Cross-linking maintains the polyphenols within the SiO_2, which endows the material with mechanical stability.

The SiO_2/polyphenol matrices demonstrated to adsorb Pb(II), Cr(III), and Cr(VI) from aqueous solutions. Media pH showed to be an important parameter in the polyphenols quelating activity, being necessary the adjustment to acidic pH. This probed to be an advantage for acidic wastewater such as Cr(III) containing tannery wastewater where the hybrid materials could be applied straightforward without conditioning the sample. After sorption, recovery of the metal could be achieved in strong acidic media and the remaining material mainly consists in SiO_2 and can be easily dispose without further treatment. Metal adsorption followed a charge associated spontaneous reaction as the main mechanism. Yerba mate dust has no commercial application for human consumption, therefore is expected that it will remain a waste of the Yerba mate industry and therefore could be considered a low-cost adsorbent.

Acknowledgements

M.P.P. is grateful for her undergraduate fellowship granted by Universidad de Buenos Aires. A.M.M. is grateful for her doctoral fellowship granted by Agencia Nacional de Promoción Científica y Técnica. This work was supported with grants from Universidad de Buenos Aires (UBACYT B049 and 20020090300085). Authors would like to thank J. Nesterzak for his technical assistance.

Appendix A. Supplementary data

Supplementary data associated with this article can be found, in the online version, at http://dx.doi.org/10.1016/j.colsurfb.2012.08.015.

References

[1] S.E. Manahan, Introducción a La Química Ambiental, Reverté, Barcelona, España, 2007.
[2] G.M. Gadd, J. Chem. Technol. Biotechnol. 84 (2009) 13.
[3] S.E. Bailey, T.J. Olin, R.M. Bricka, D.D. Adrian, Water Res. 33 (1999) 2469.
[4] G. Crini, Bioresour. Technol. 97 (2006) 1061.
[5] P. Miretzky, A. Saralegui, A. Fernández Cirelli, Chemosphere 62 (2006) 247.
[6] S. Bellú, S. García, J.C. González, A.M. Atria, L.F. Sala, S. Signorella, Sep. Sci. Technol. 43 (2008) 3200.
[7] M.E. Fernandez, G.V. Nunell, P.R. Bonelli, A.L. Cukierman, Bioresour. Technol. 101 (2010) 9500.
[8] M.M. Areco, M. dos Santos Afonso, Colloids Surf. B 81 (2010) 620.
[9] Y. Nakano, K. Takeshita, T. Tsutsumi, Water Res. 35 (2001) 496.
[10] M. Özacar, İ.A. Şengil, Colloids Surf. A 229 (2003) 85.
[11] X.-M. Zhan, X. Zhao, Water Res. 37 (2003) 3905.
[12] J. Beltrán-Heredia, J. Sánchez-Martín, A. Delgado-Regalado, C. Jurado-Bustos, J. Hazard. Mater. 170 (2009) 43.
[13] T.S. Anirudhan, S.R. Rejeena, A.R. Tharun, Colloids Surf. B 93 (2012) 49.
[14] G.J. Copello, A.M. Mebert, M. Raineri, M.P. Pesenti, L.E. Diaz, J. Hazard. Mater. 186 (2011) 932.
[15] V. Breguet, J. Boucher, F. Pesquet, V. Vojinovic, U. von Stockar, I.W. Marison, Water Res. 42 (2008) 1606.
[16] D. Avnir, T. Coradin, O. Lev, J. Livage, J. Mater. Chem. 16 (2006) 1013.
[17] C. Contreras, G. de la Rosa, J.R. Peralta-Videa, J.L. Gardea-Torresdey, J. Hazard. Mater. 133 (2006) 79.
[18] G.J. Copello, F. Varela, R. Martinez Vivot, L.E. Diaz, Bioresour. Technol. 99 (2008) 6538.
[19] R. Filip, P. Lopez, G. Giberti, J. Coussio, G. Ferraro, Fitoterapia 72 (2001) 774.
[20] C.I. Heck, E.G. de Mejia, J. Food Sci. 72 (2007) 138.
[21] L. Deladino, P.S. Anbinder, A.S. Navarro, M.N. Martino, Carbohydr. Polym. 71 (2008) 126.
[22] R Development Core Team, R: A Language and Environment for Statistical Computing, R Foundation for Statistical Computing, Vienna, Austria, 2009.
[23] M.F. Desimone, S.B. Matiacevich, M.d.P. Buera, L.E. Diaz, Enzyme Microb. Technol. 42 (2008) 583.
[24] G.S. Alvarez, M.L. Foglia, G.J. Copello, M.F. Desimone, L.E. Diaz, Appl. Microbiol. Biotechnol. 82 (2009) 639.
[25] T. Nakagawa, M. Soga, J. Non-Cryst. Solids 260 (1999) 167.
[26] B. Orel, R. Jese, U.L. Stangar, J. Grdadolnik, M. Puchberger, J. Non-Cryst. Solids 351 (2005) 530.
[27] M.-L. Josien, N. Fuson, J.-M. Lebas, T.M. Gregory, J. Chem. Phys. 21 (1953) 331.
[28] G.J. Copello, R.E. Garibotti, F. Varela, M.V. Tuttolomondo, L.E. Diaz, J. Braz. Chem. Soc. 22 (2011) 790.
[29] R.K. Iler, The Chemistry of Silica, J Wiley, New York, 1979.
[30] R. Elangovan, L. Philip, K. Chandraraj, J. Hazard. Mater. 152 (2008) 100.
[31] M.A. Morsy, M.M. Khaled, J. Agric. Food Chem. 49 (2001) 683.
[32] J.C. González, S.I. García, S. Bellú, A.M. Atria, J.M.S. Pelegrín, A. Rockenbauer, L. Korecz, S. Signorella, L.F. Sala, Polyhedron 28 (2009) 2719.
[33] P. Suksabye, A. Nakajima, P. Thiravetyan, Y. Baba, W. Nakbanpote, J. Hazard. Mater. 161 (2009) 1103.
[34] Y.S. Ho, G. McKay, Water Res. 34 (2000) 735.
[35] C. Cheung, J. Porter, G. Mckay, Water Res. 35 (2001) 605.
[36] H. Teng, C.-T. Hsieh, Ind. Eng. Chem. Res. 38 (1998) 292.
[37] S. Kuo, E.G. Lotse, Soil Sci. 116 (1973).
[38] M. Hadi, M.R. Samarghandi, G. McKay, Chem. Eng. J. 160 (2010) 408.
[39] H. Akaike, IEEE Trans. Automatic Control 19 (1974) 716.
[40] C.M. Hurvich, C.-L. Tsai, Biometrika 76 (1989) 297.
[41] E.-J. Wagenmakers, S. Farrell, Psychon. Bull. Rev. 11 (2004) 192.
[42] Y.-S. Ho, J. Hazard. Mater. 136 (2006) 681.
[43] G.J. Copello, L.E. Diaz, V. Campo Dall' Orto, J. Hazard. Mater. 217–218 (2012) 374.
[44] S.-Y. Suen, J. Chem. Technol. Biotechnol. 65 (1996) 249.
[45] S.S. Barton, J. Colloid Interface Sci. 158 (1993) 64.
[46] A.M. El-Kamash, A.A. Zaki, M.A. El Geleel, J. Hazard. Mater. 127 (2005) 211.
[47] D. Kumar, L.K. Pandey, J.P. Gaur, Colloids Surf. B 81 (2010) 476.
[48] J. Toth, Adsorption: Theory, Modeling and Analysis, Marcel Dekker, New York, 2002.
[49] B. Singha, S.K. Das, Colloids Surf. B 84 (2011) 221.
[50] M.G. da Fonseca, M.M. de Oliveira, L.N. Arakaki, J.G. Espinola, C. Airoldi, J. Colloid Interface Sci. 285 (2005) 50.
[51] P.D. Saha, S. Chakraborty, S. Chowdhury, Colloids Surf. B 92 (2012) 262.
[52] M. McDonald, I. Mila, A. Scalbert, J. Agric. Food Chem. 44 (1996) 599.